Electronic Supplementary Material (ESI) for Journal of Materials Chemistry A.
This journal is © The Royal Society of Chemistry 2023

Supporting Information

Thermal-Reconstruction Engineered Titanium-Based Gas Diffusion Electrodes for Energy-Saving Hydrogen Hydrometallurgy

Anbang Zheng [1, 2, #], Yufeng Su [1, 2, #], Songtao Lin [1, 2], Yuchen Wang [1, 2], Zhilin Li [1, 2], Zhengping Zhang [1, 2*], Feng Wang [1,2 *]*

[1] State Key Laboratory of Chemical Resource Engineering, Beijing Key Laboratory of Electrochemical Process and Technology for Materials, Beijing University of Chemical Technology, Beijing 100029, P. R. China.

[2] Beijing Advanced Innovation Center for Soft Matter Science and Engineering, Beijing University of Chemical Technology, Beijing 100029, P. R. China.

* Corresponding email: zhangzhengping@mail.buct.edu.cn (Z. Zhang); lizl@mail.buct.edu.cn (Z. Li); wangf@mail.buct.edu.cn (F. Wang);

# These authors contributed equally to this work.

1. Material and methods

1.1 Materials

All materials used in this work had been listed in the following: zinc sulfate hexahydrate ($ZnSO_4 \cdot 6H_2O$, AR), copper sulfate pentahydrate ($CuSO_4 \cdot 5H_2O$, AR), sulfuric acid (H_2SO_4, AR), ethanol (CH_3CH_2OH, GR) and gelatin (AR) was purchased from Sinopharm Chemical Reagent Co., Ltd. $SnCl_2$ ($\geqslant$99%) and $H_2C_2O_4$ (99.99%) were purchased from Shanghai Aladdin Biochemical Technology Company Limited. Titanium butoxide ($C_{16}H_{36}O_4Ti$, AR) was brought from Shanghai Macklin Biochemical Co., Ltd. H_2PtCl_6 was obtained from J&K Scientific Ltd. Teflon solution (60% wt.% in H_2O) was purchased from Suzhou Sinero Technology Co., Ltd. Carbon cloth with a microporous layer was obtained from Ce Tech Co., Ltd. Titanium felt was purchased from Baoji Yongheshun Titanium Industry Co., Ltd. Aluminum plate serving as cathode was obtained from Shenzhen Kaisheng Hardware Mould Co., Ltd. 316 stainless steel serving as cathode was brought from Beijing Hongyan Metal Material Co., Ltd. Ultrapure water (18.2 MΩ cm) was obtained from a water purification system (Beyond-q) without further purification.

1.2 Materials Characterization

The structures and morphologies of the synthesized electrocatalysts were observed by powder X-ray diffraction (XRD), scanning electron microscope (SEM), and transmission electron microscopy (TEM). XRD equipped with Cu *K*α radiation at λ = 1.54 Å on a Philips Xpert X-ray diffractometer. SEM characterization was performed with a FE-JSM-6701F microscope. TEM characterization was performed with a JEOL TEM 2010 microscope. The samples were also studied by a transmission electron microscope (TEM, JEOL F200) and by energy dispersive X-ray spectroscopic (EDX)

mapping. The compositions loading was determined by inductively coupled plasma (ICP)-optical emission spectroscopy using a PerkinElmer 2000 DV ICP-OES instrument. X-band electron paramagnetic resonance (EPR) measurement was performed at room temperature using a Bruker A300-10/12 spectrometer. The microscopic photographs of electrodes were characterized by optical microscope (E3ISPM20000KPA). Element ratio on electrode surface was measured by X-ray fluorescence spectrometer (Shimadzu XRF-1800).

1.3 Electrochemical Testing

The CV, LSV, EIS experiments were conducted in a cell with three electrodes using CHI 660E (Shanghai Chenhua Instrument Corporation, China) control system. In the three-electrode system, the reference electrode (Hg/Hg_2Cl_2/1M KCl) was calibrated with respect to RHE using the equation $E_{RHE} = E_{Hg/Hg_2Cl_2} + (0.059 \times pH)$. Electrochemical surface area (ECSA) was measured by CV measurement, which was done with 100 mV s^{-1} scan rate from 0.05 V to 1.2 V with N_2 saturated 1.5 M H_2SO_4 electrolyte. The LSV and EIS curves for HOR were measured in 1.5 M H_2SO_4. The LSV curves was measured by scan rate of 1 mV s^{-1} from –0.02 V to 0.21 V in a H_2 saturated environment after 3,000 potential cycles (from –0.06 V to 0.44 V, scan rate of 100 mV/sec). Electrochemical Impedance Spectroscopy (EIS) were performed in the frequency range 10^5 Hz to 10^{-1} Hz with a constant AC voltage with the overpotential of 30 mV. Chronopotentiometry experiment which was simulated the industrial operating condition that the current was 0.8 A for 8 h also was carried out by the DC source meter (M8811).

The electrochemical surface area (ECSA) was calculated by measuring the areas of H desorption between 0.05 V and 0.4 V after the deduction of the double-layer region by use of the following equation:

$$\mathrm{ECSA} = \frac{Q\mathrm{H}}{[\mathrm{Pt}] \times 0.21}$$

Where [Pt] represents the platinum loading (mg cm^{-2}) on the electrode, Q_H depicts the charge for H-desorption (mC cm^{-2}) and 0.21 is the charge required to oxidize a monolayer of H_2 on clean Pt.

2. Results and discussion

Table S1. The Pt content in Pt-SnTi, Pt-Sn, and Pt-Ti measured by ICP.

	Pt-Sn	Pt-SnTi	Pt-Ti
Pt loading (mg_{Pt} cm^{-2})	1.20	1.22	1.20

Table S2 The determined element composition and content of Pt-SnTi, Pt-Ti and Pt-Sn obtained from XPS measurement.

Elements	PtTi	PtSnTi	PtSn
Pt(at.%)	2.76	8.04	16.59
Sn(at.%)	/	2.82	2.43
Ti(at.%)	25.36	21.50	5.68
O (at.%)	71.88	67.64	75.30

Table S3 The relative contents and positions of three Pt moieties and two O moieties of the above three samples compared with pure Pt coating.

Samples	Functionality (% of total Pt $4f_{7/2}$)					
	Pt^{4+}	Position (eV)	Pt^{2+}	Position (eV)	Pt^{0}	Position (eV)
Pt-Sn	16.7	73.8	44.8	71.5	38.5	70.6
Pt-SnTi	35.0	74.5	33.8	71.9	31.2	71.0
Pt-Ti	49.0	74.6	26.2	72.3	24.8	71.0
Pt	19.4	74.9	54.7	72.1	25.9	71.5
Samples	Functionality (% of total O 1*s*)					
	O1	Position (eV)	O2	Position (eV)		
Pt-Sn	20.3	529.7	79.7	532.4		
Pt-SnTi	66.4	529.8	33.6	531.7		
Pt-Ti	67.9	529.8	32.1	531.6		

Table S4 The fitted parameters of the EIS data of Pt-Ti and Pt-SnTi.

	R_{sol} (ohm)	CPE-T, Q_{ct}	CPE-P, n	R_{ct} (ohm)	CPE-T, Q_1	CPE-P, n	R_1 (ohm)
Pt-Ti	1.34	9.68×10^{-2}	0.7037	5.957	5.08×10^{-2}	0.812	7.8×10^{8}
Pt-SnTi	1.42	4.75×10^{-2}	0.8664	0.445	5.41×10^{-2}	0.807	1.9×10^{11}

Table S5 Metal electrowinning performance of the Pt-SnTi GDE.

Performance parameters	Cu electrowinning	Zn electrowinning
Average cell voltage (V)	0.58	1.33
Average current efficiency (%)	99.2	91.9
Average Power consumption (kWh/t)	491	1187

Table S6 Element content of metal plates electrodeposited by the Pt-SnTi GDE measured by ICP.

	Pt (mg/kg)	Sn (mg/kg)	Ti (mg/kg)
Cu electrowinning	0.03	0.03	0.06
Zn electrowinning	0.00	0.01	0.12

Table S7 XRF of the Pt-SnTi GDE before and after operations.

Element	Pt	Sn	Ti	F
Initial (wt%)	1.87	0.24	58.58	39.31
After operation (wt%)	1.83	0.19	61.48	36.50

Table S8. The relative contents of Pt moieties in the Pt-SnTi GDE before and after operations.

Samples	Functionality (% of total Pt $4f_{7/2}$)		
	Pt^{4+}	Pt^{2+}	Pt^{0}
Pt-SnTi before operation	35.0	33.8	31.2
Pt-SnTi after operation	19.4	54.7	26.3

Table S9 The contents of industrial electrolyte in this work measured by ICP.

Element (g/L)							
Zn	~70	H^+	~140	Mn	0.12	Fe	0.79
Co	0.06	Ni	~1	Cu	~0.20	F	53.42
Cl	~0.00	Ge	~0.00	As	~0.10	Cd	~0.80
Sb	~0.00	COD	41.19				

Table S10 Polarization parameters and fitted equivalent circuit parameters of Ti felt and carbon cloth.

Sample	E_{corr} (mV)	j_{corr} ($\mu A \cdot cm^{-2}$)	R_s (Ω)	CPE_0	R_c (Ω)
Ti felt	81	6.61	1.99	1.05×10^{-4}	2.61×10^{5}
Carbon cloth	−134	50.12	1.209	3.745×10^{-5}	2.251×10^{4}

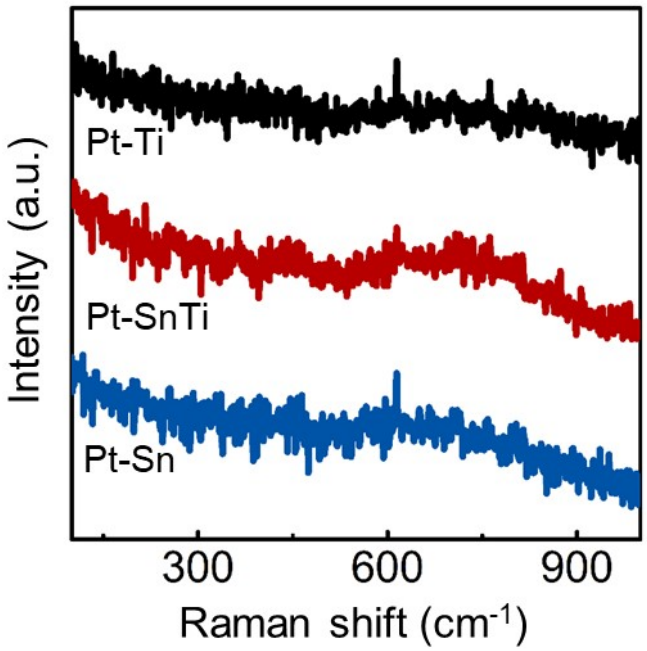

Fig. S1 Raman spectra of Pt-Ti, Pt-SnTi and Pt-Sn.

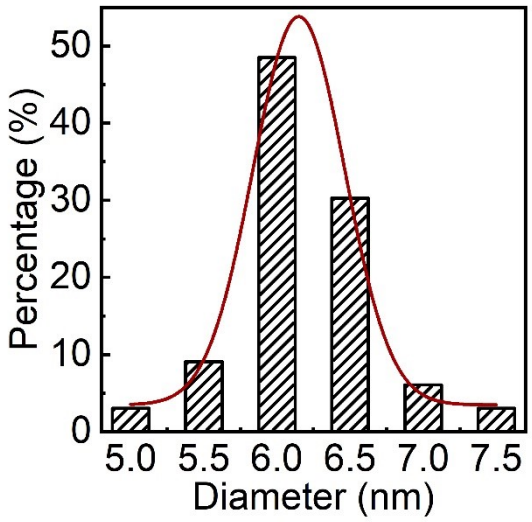

Figure S2. The Pt particle size distribution of Pt-SnTi.

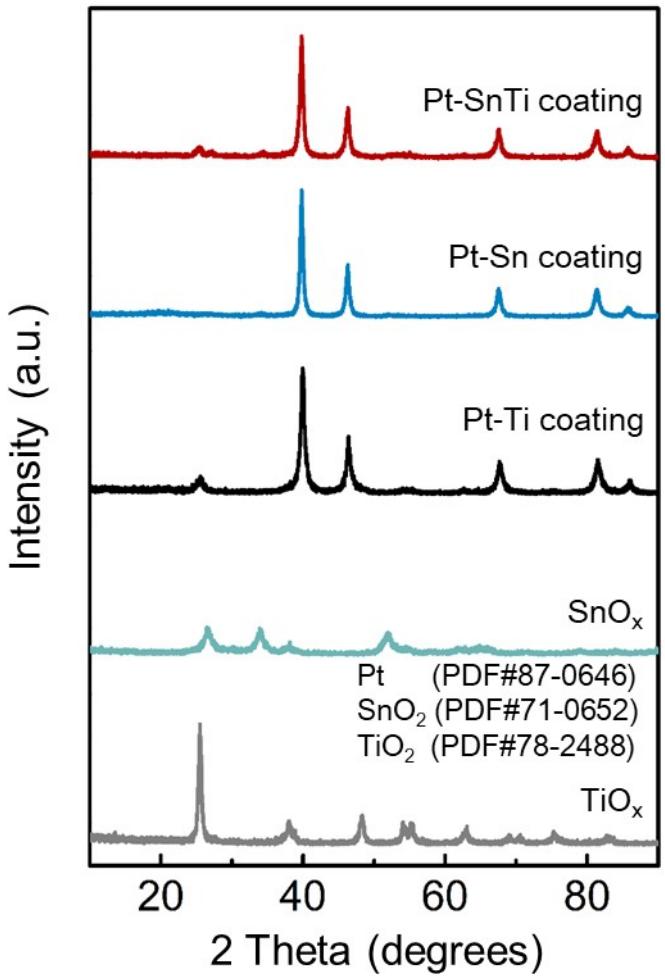

Fig. S3 XRD patterns of calcinated powders derived from the Pt-SnTi, Pt-Sn, Pt-Ti coatings, compared with the calcinated SnO_x and TiO_x.

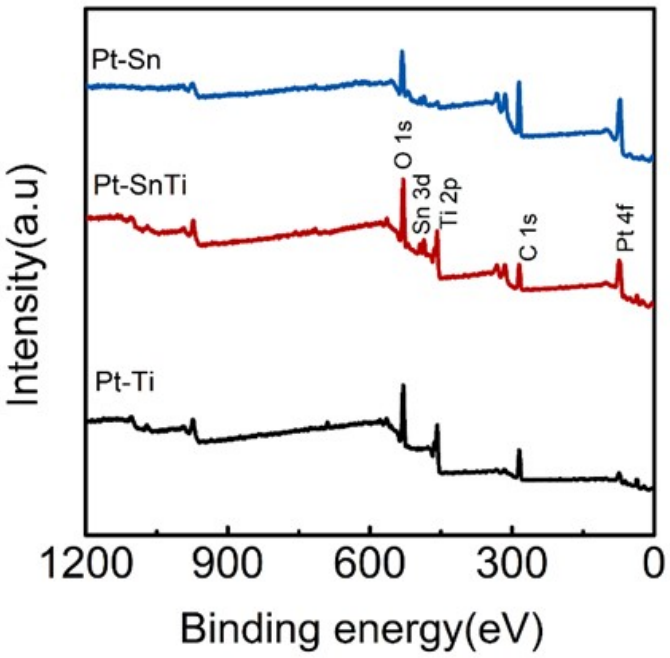

Fig. S4 XPS survey spectra of Pt-SnTi, Pt-Sn and Pt-Ti.

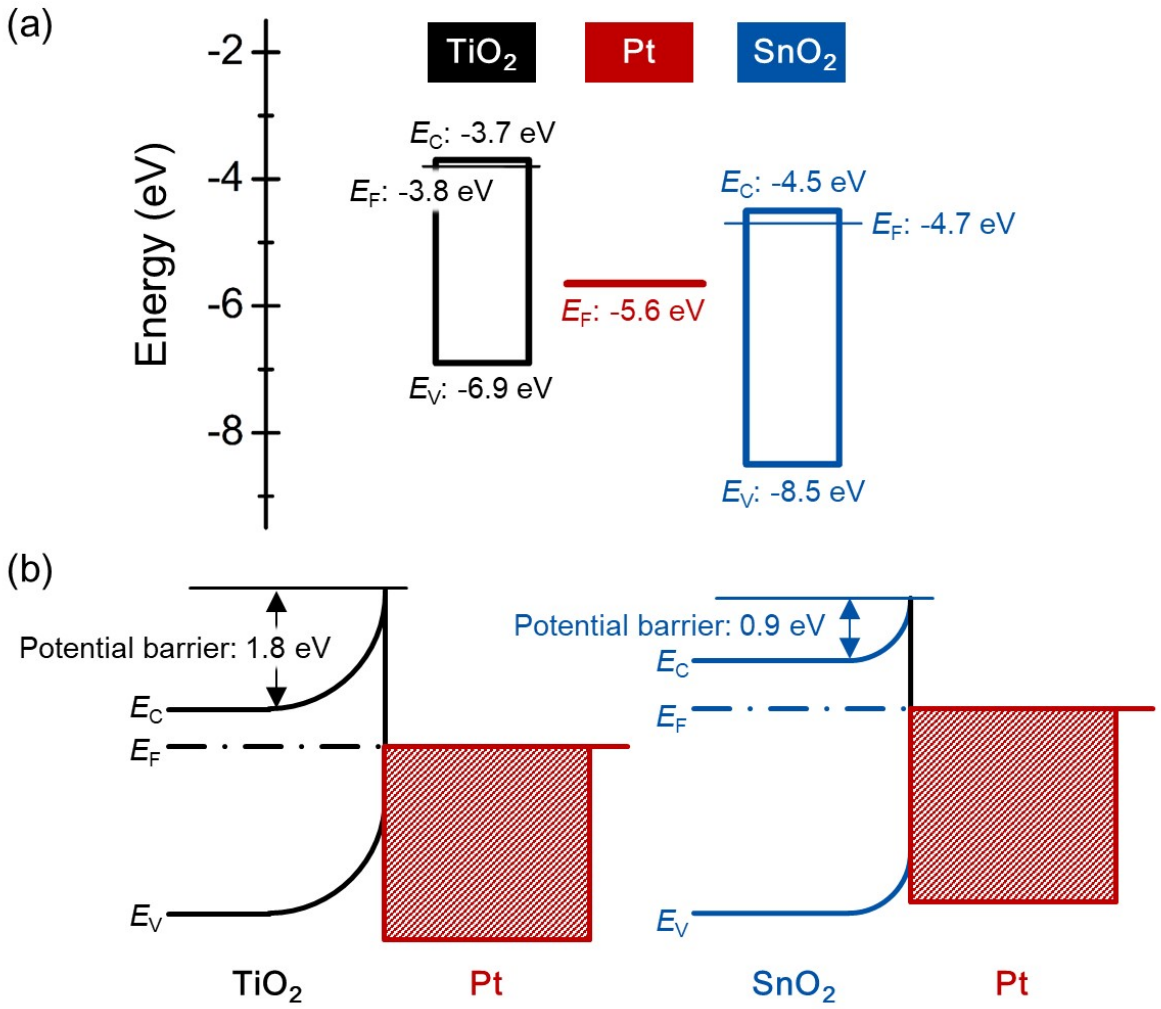

Fig.S5. (a) Schematic band energy alignments of TiO_2, SnO_2 and Pt. (b) Schematic diagrams of energy band bending and electron transition at Pt-TiO_x and Pt-SnO_x heterojunctions.

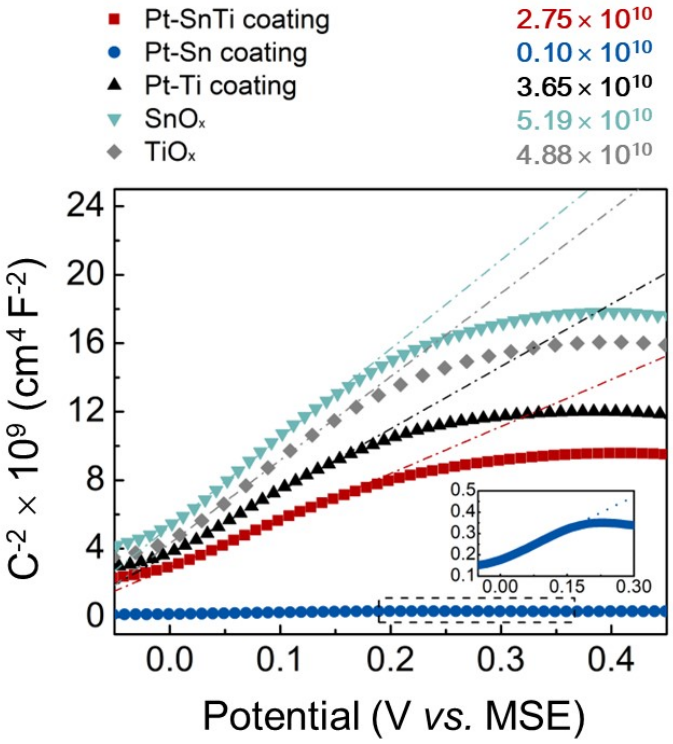

Fig. S6 Mott−Schottky plots of calcinated powders derived from the Pt-SnTi, Pt-Sn, Pt-Ti coatings, compared with the calcinated SnO_x and TiO_x.

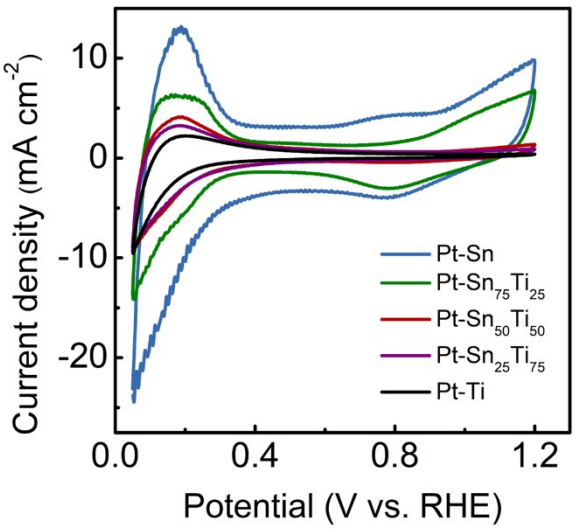

Fig. S7 CV curves for ECSA with 100 mV s^{-1} scan rate from 0.05 V to 1.2 V with N_2 saturated 1.5 M H_2SO_4 electrolyte.

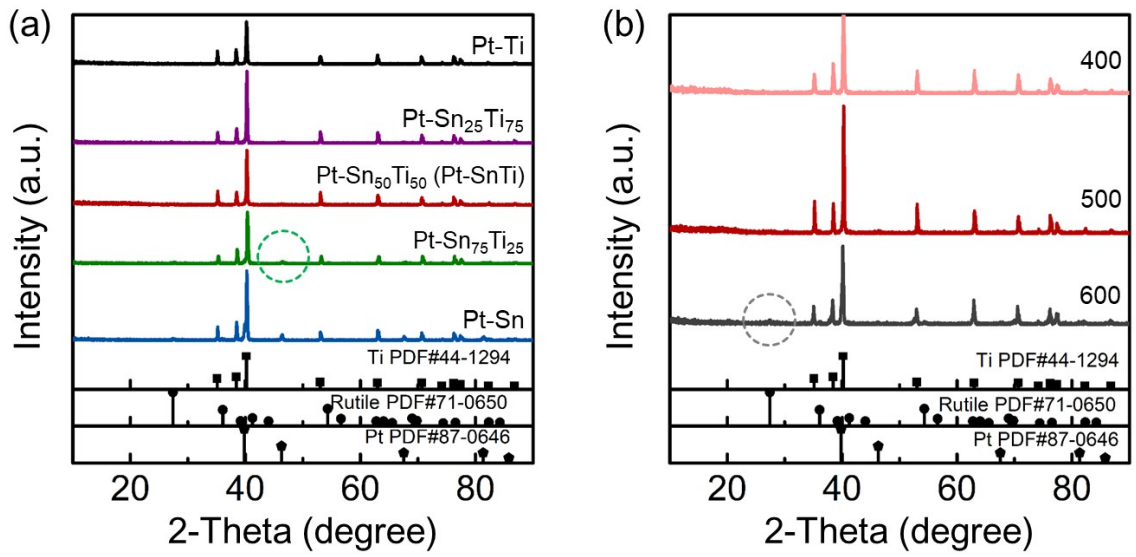

Fig. S8 (a) XRD patterns of Pt-Sn, Pt-Ti, and Pt-SnTi with different Sn/Ti ratios (including Pt-$Sn_{75}Ti_{25}$, Pt-$Sn_{50}Ti_{50}$, and Pt-$Sn_{25}Ti_{75}$). (b) XRD patterns of Pt-SnTi (Sn/Ti ratios of 50:50) with different-temperature (400, 500, 600 °C) treatment.

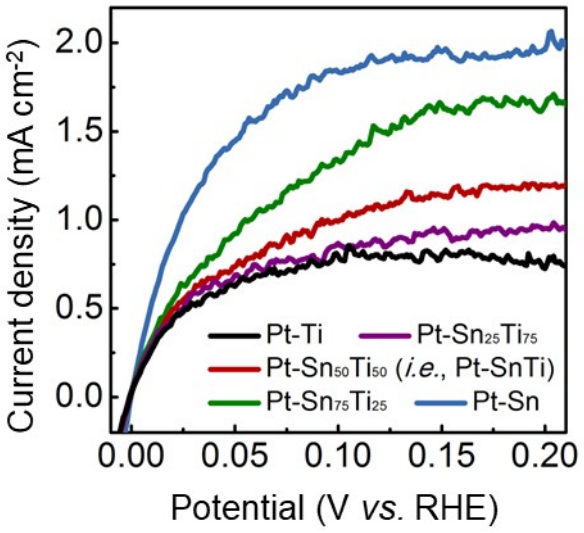

Fig. S9 The initial LSV curves of Pt-Sn, Pt-Ti, and Pt-SnTi with different Sn/Ti ratios (including Pt-$Sn_{75}Ti_{25}$, Pt-$Sn_{50}Ti_{50}$, and Pt-$Sn_{25}Ti_{75}$).

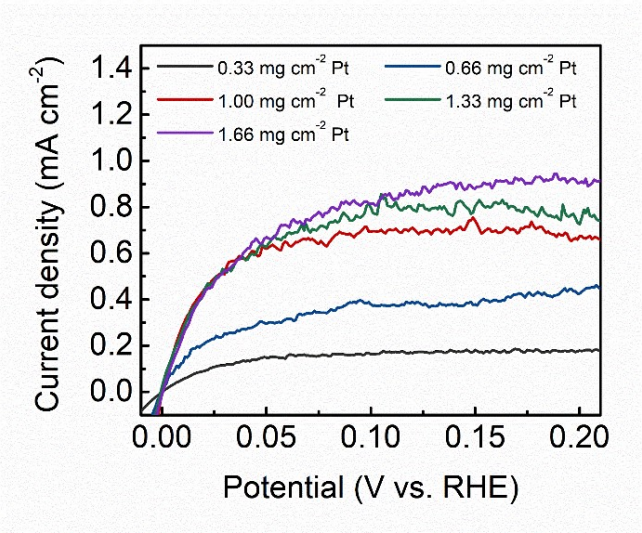

Figure S10. The HOR LSV curves of Pt-$Sn_{50}Ti_{50}$ with different Pt contents.

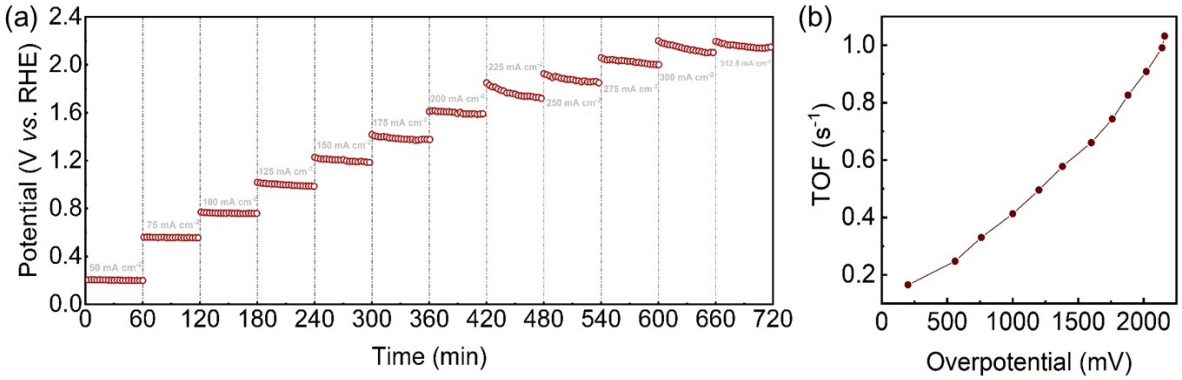

Figure S11. (a) Chronopotentiometric curves recorded at different current denisties, and (b) the corresponding calculated TOFs of the Pt-SnTi GDEs.

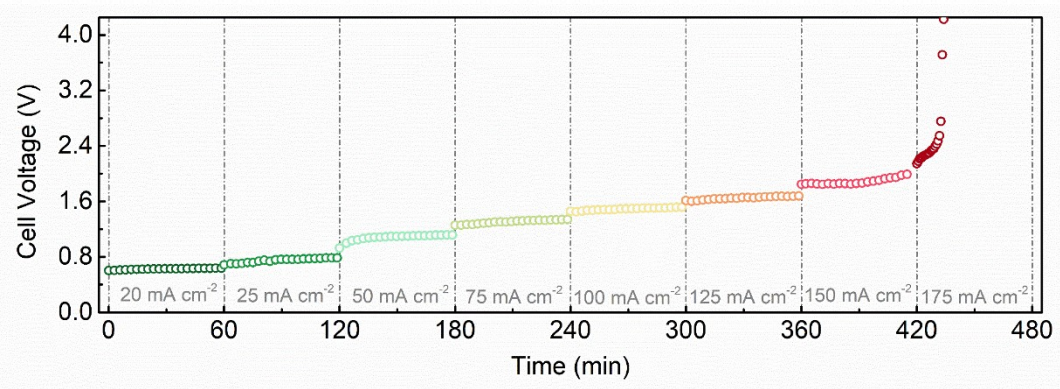

Figure S12. The cell voltages - time curve for copper electrowinning by using the Pt-SnTi GDE at different current densities.

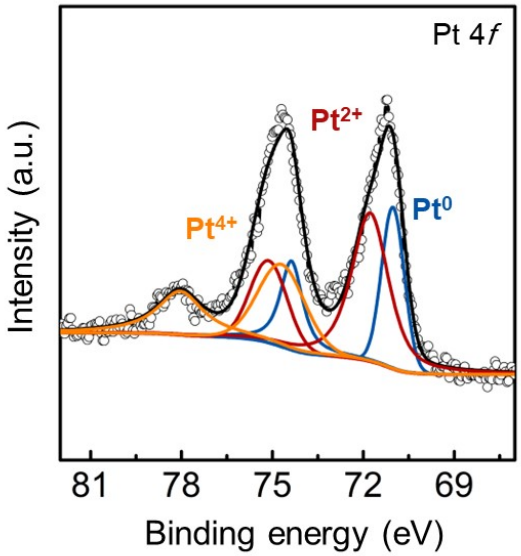

Fig. S13 High resolution Pt 4*f* XPS spectra of Pt-SnTi after operation.

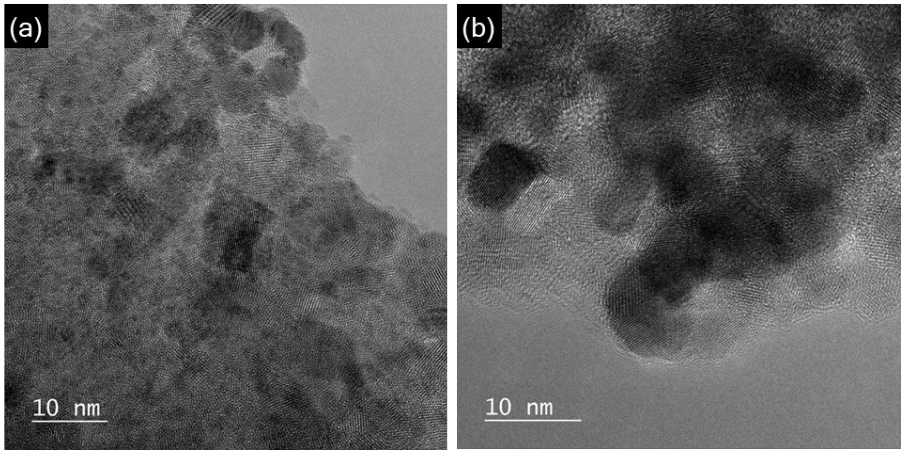

Figure S14. HR-TEM images of Pt-SnTi (a) before and (b) after operation.

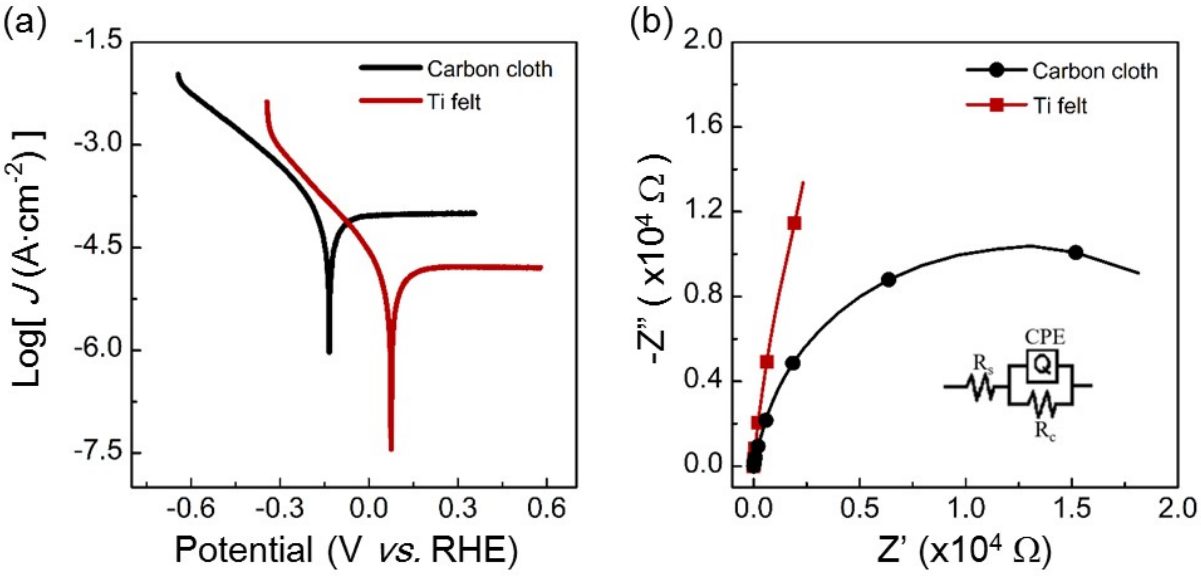

Fig. S15 (a) Potentiodynamic polarization curves (a scan rate of 1 mV s^{-1}) and (b) Nyquist plots (1.3 V *vs.* RHE) of the carbon cloth and the Ti felt in 1.5 M H_2SO_4 solution.

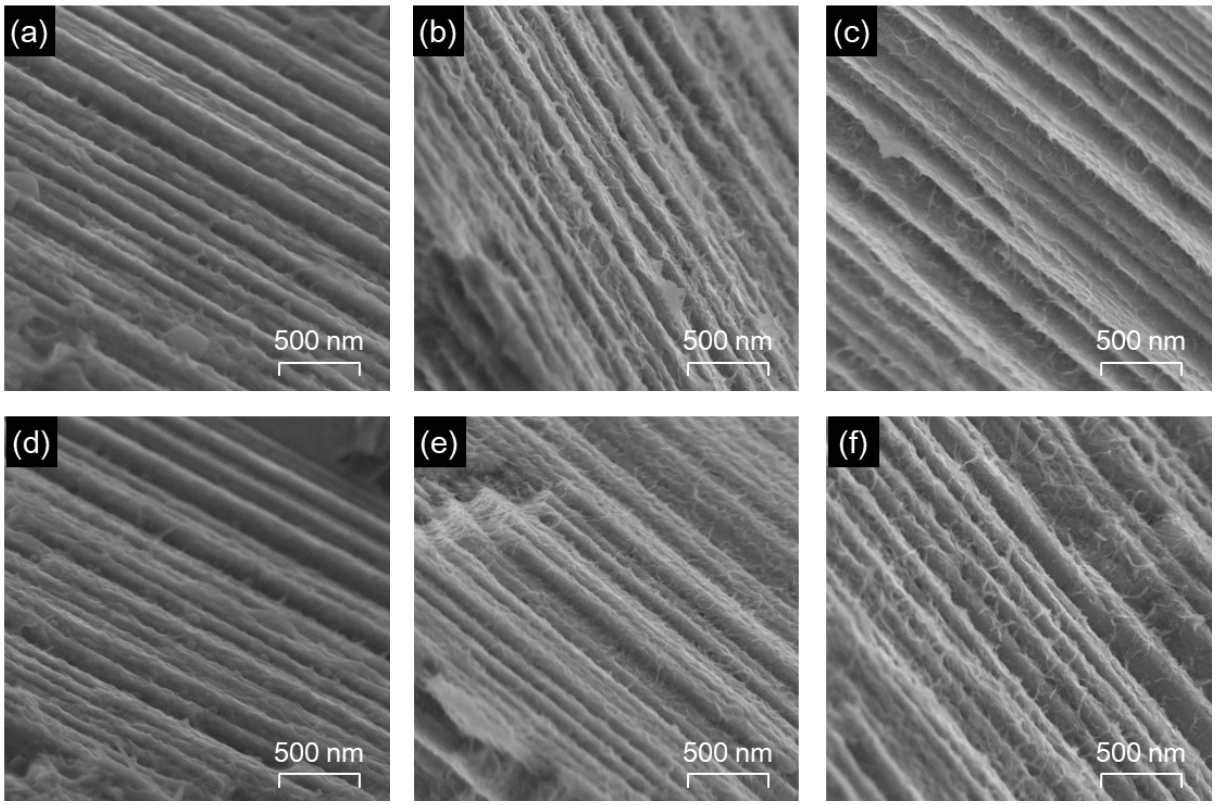

Fig. S16 SEM images of the stripped Zn for the (a) 1st, (b) 7th, (c) 8th, (d) 19th, (e) 20th, (f) 28th time.

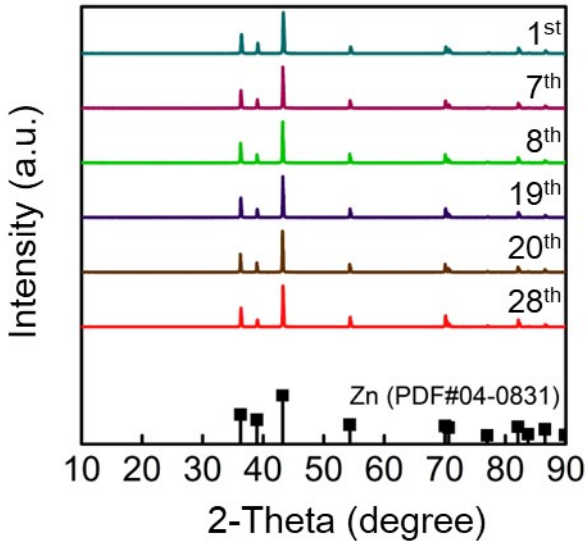

Fig. S17 XRD patterns of the stripped Zn at different times.